



MMM11 - symposium O

Phase-field modelling of microstructure evolution during complex thermal cycles : application to martensitic steels

Jules L'HOSTIS*, Marie-Noëlle AVETTAND-FÈNOËL, Manon
BONVALET-ROLLAND and Ludovic THUINET

Univ. Lille, CNRS, INRAE, Centrale Lille, UMR 8207 - UMET - Unité Matériaux et
Transformations, F-59000 Lille, France

September 26th, 2024



*jules.l_hostis@centralelille.fr

Contents

1 Introduction

2 Phase-field method

- Order parameters
- Energy of the system
- Coupling strategy

3 Results

- Benchmark simulations
- Simulations using the experimental cooling curve from WAAM

4 Conclusion

Contents

1 Introduction

2 Phase-field method

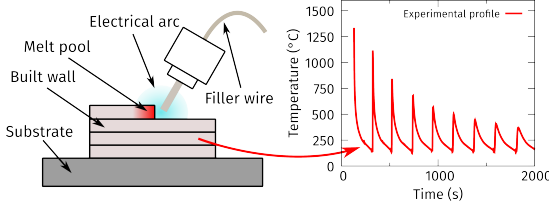
- Order parameters
- Energy of the system
- Coupling strategy

3 Results

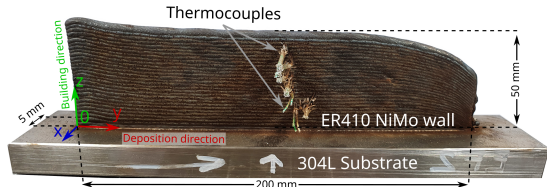
- Benchmark simulations
- Simulations using the experimental cooling curve from WAAM

4 Conclusion

Introduction



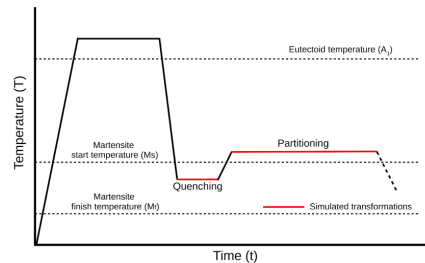
Wire-arc additive manufacturing (WAAM) and associated thermal cycle.



ER410 NiMo part built by WAAM and instrumented with thermocouples.

Context

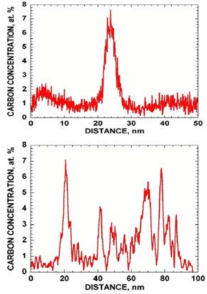
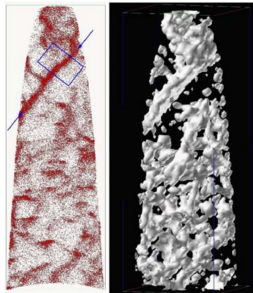
- Industrial processes: complex thermal treatments (ex: WAAM).
- Phase-field models are used to predict phase transformations. Often used for simple (and simplified) thermal cycles such as quenching & partitioning (Q&P).



Phase field simulation of Q & P treatment from Kubendran Amos et al.¹

¹P. G. Kubendran Amos et al., Computational Materials Science 2019, 159, 281–296

Introduction



Carbon segregation in martensite (APT) after quenching
from Sherman et al.²

- Some extent of carbon partitioning can occur *during* the quenching.
- The cooling speed can affect these segregations.

Objectives

- Phase-field model for **simultaneous** martensitic transformation and carbon diffusion during WAAM of a martensitic stainless steel (ER410 NiMo³).

²D. H. Sherman et al., *Metallurgical and Materials Transactions A* **2007**, 38, 1698–1711

³Fe + 0.11 at.%C, 13.4 at · %Cr and 4.4 at · %Ni + minor elements not taken into account.

Contents

1 Introduction

2 Phase-field method

- Order parameters
- Energy of the system
- Coupling strategy

3 Results

- Benchmark simulations
- Simulations using the experimental cooling curve from WAAM

4 Conclusion

Selection of order parameters

Non-conserved order parameters

- 2 order parameters (OPs) η_p for 2 martensite variants in 2D.

Conserved order parameters

- 1 conserved OP X_c for carbon content.

Selection of order parameters

Non-conserved order parameters

- 2 OPs η_p for 2 martensite variants in 2D.
- Allen-Cahn type equation:

$$\frac{\partial \eta_p}{\partial t_m^*} = - \left(\frac{\delta G}{\delta \eta_p} \right) + \xi^* \quad (1)$$

with ξ^* a noise term.

Conserved order parameters

- 1 conserved OP X_C for carbon content.
- Cahn-Hilliard type equation:

$$\frac{\partial X_C}{\partial t_d^*} = \text{div}^* \left(M^* \nabla^* \frac{\partial G_v^{\text{chem}*}}{\partial X_C} \right) \quad (3)$$

with M^* the mobility of carbon.

Selection of order parameters

Non-conserved order parameters

- 2 OPs η_p for 2 martensite variants in 2D.
- Allen-Cahn type equation:

$$\frac{\partial \eta_p}{\partial t_m^*} = - \left(\frac{\delta G}{\delta \eta_p} \right) + \xi^* \quad (1)$$

with ξ^* a noise term.

- Temporal reduction : $t_m^* = t_m / t_0^m$ with

$$t_0^m = \frac{1}{\Delta G_0 L} \quad (2)$$

with L the kinetic coefficient of martensite.

(*) denotes the dimensionless form. ΔG_0 is the reference and a_0 the reference length.

Conserved order parameters

- 1 conserved OP X_C for carbon content.
- Cahn-Hilliard type equation:

$$\frac{\partial X_C}{\partial t_d^*} = \text{div}^* \left(M^* \nabla^* \frac{\partial G_v^{\text{chem}*}}{\partial X_C} \right) \quad (3)$$

with M^* the mobility of carbon.

- Temporal reduction : $t_d^* = t_d / t_0^d$ with

$$t_0^d = \frac{a_0^2}{\Delta G_0 M_0} \quad (4)$$

with M_0 the reference carbon mobility.

Selection of order parameters

Non-conserved order parameters

- 2 OPs η_p for 2 martensite variants in 2D.
- Allen-Cahn type equation:

$$\frac{\partial \eta_p}{\partial t_m^*} = - \left(\frac{\delta G}{\delta \eta_p} \right) + \xi^* \quad (1)$$

with ξ^* a noise term.

- Temporal reduction : $t_m^* = t_m / t_0^m$ with

$$t_0^m = \frac{1}{\Delta G_0 L} \quad (2)$$

with L the kinetic coefficient of martensite.

(*) denotes the dimensionless form. ΔG_0 is the reference and a_0 the reference length.

Main assumption: $t_0^m \ll t_0^d$.

Conserved order parameters

- 1 conserved OP X_C for carbon content.
- Cahn-Hilliard type equation:

$$\frac{\partial X_C}{\partial t_d^*} = \text{div}^* \left(M^* \nabla^* \frac{\partial G_v^{\text{chem}*}}{\partial X_C} \right) \quad (3)$$

with M^* the mobility of carbon.

- Temporal reduction : $t_d^* = t_d / t_0^d$ with

$$t_0^d = \frac{a_0^2}{\Delta G_0 M_0} \quad (4)$$

with M_0 the reference carbon mobility.

Energy of the system

Energy of the system:

$$G = \int_V G_v^{\text{chem}} + G_v^{\text{grad}} + G_v^{\text{elas}} dV \quad (5)$$

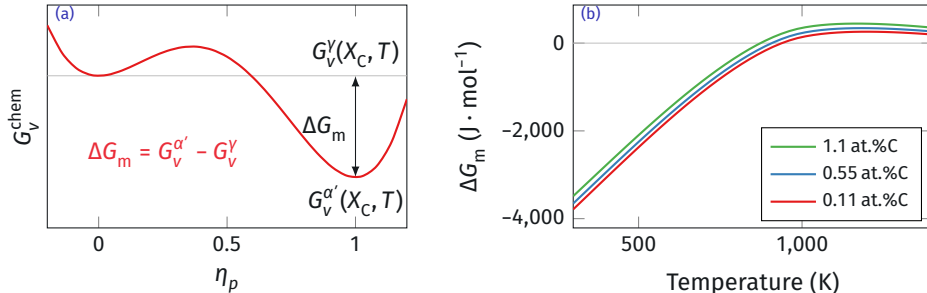
with :

- G_v^{chem} : chemical energy, based on a LANDAU potential⁴.
- G_v^{elas} : elastic energy, based on the microelasticity theory⁵. **2 cases depending on boundary conditions:**
 - *clamped* ($\bar{\varepsilon} = 0$)
 - *stress free* ($\bar{\sigma} = 0$).

⁴H. K. Yeddu et al., *Acta Materialia* 2012, 60, 1538–1547

⁵A. G. Khachaturyan, *Theory of Structural Transformations in Solids*, 1983

CALPHAD coupling of the chemical energy



(a) LANDAU type chemical energy and (b) CALPHAD-based energy potentials.

$$G_v^{\text{chem}}(\eta_p, X_C, T) = \frac{A}{2} \left(\sum_p \eta_p^2 \right) - \frac{B}{3} \left(\sum_p \eta_p^3 \right) + \frac{C}{4} \left(\sum_p \eta_p^2 \right)^2 + G_v^Y(X_C, T) \quad (6)$$

$$\begin{cases} A &= 32\Delta G_b \\ B &= 3A - 12\Delta G_m \\ C &= 2A - 12\Delta G_m \end{cases}$$

ΔG_b is the nucleation barrier and ΔG_m the chemical driving force: $\Delta G_m = G_v^{\alpha'}(T, X_C) - G_v^Y(T, X_C)$.

$G_v^\phi(T, X_C)$ calculated with the CALPHAD formalism and an open source database⁶.

This dependency introduces the coupling between the evolution of martensite and carbon content.

⁶W. Liu et al., *Calphad* 2020, 69, 101763

Heterogeneous mobility of carbon

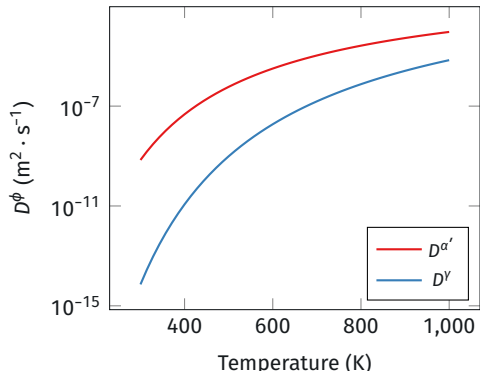
The heterogeneous mobility of carbon is determined by

$$M(\mathbf{r}, t) = M^{\alpha'}(T) \left(\sum_p \eta_p^2 \right) + M^{\gamma}(T) \left(1 - \sum_p \eta_p^2 \right) \quad (7)$$

and is linked to diffusion coefficients by

$$M^{\phi}(T) = D^{\phi}(T) \left(\frac{\partial^2 G_v^{\phi}}{\partial X_C^2} \right)^{-1} \quad (8)$$

calculated *explicitly* thanks to the CALPHAD method.

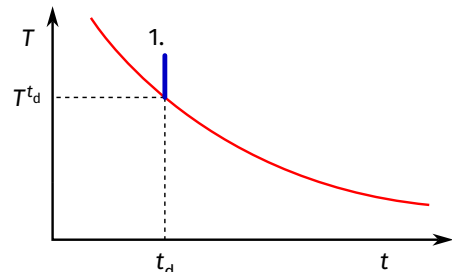


Diffusion coefficients of carbon in austenite and martensite from Kubendran Amos et al.⁷.

⁷P. G. Kubendran Amos et al., *Computational Materials Science* **2019**, 159, 281–296

Thermal treatment simulation: multi-time-step algorithm coupling strategy

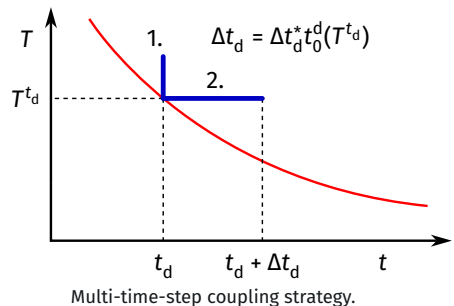
1. Displacive iterations at a certain temperature until convergence of η_p .



Multi-time-step coupling strategy.

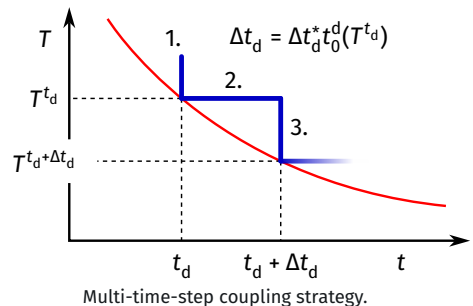
Thermal treatment simulation: multi-time-step algorithm coupling strategy

1. Displacive iterations at a certain temperature until convergence of η_p .
2. 1 diffusive iteration gives $X_C^{t_d + \Delta t_d}$.



Thermal treatment simulation: multi-time-step algorithm coupling strategy

1. Displacive iterations at a certain temperature until convergence of η_p .
2. 1 diffusive iteration gives $X_C^{t_d + \Delta t_d}$.
3. Calculation of $T^{t_d + \Delta t_d}$ from experimental curve.



Contents

1 Introduction

2 Phase-field method

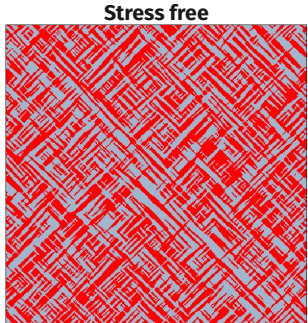
- Order parameters
- Energy of the system
- Coupling strategy

3 Results

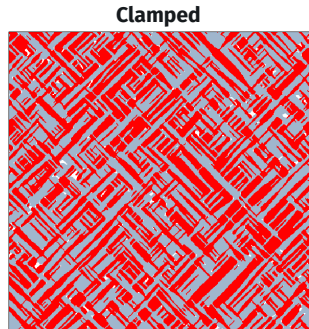
- Benchmark simulations
- Simulations using the experimental cooling curve from WAAM

4 Conclusion

Benchmark simulations: influence of boundary conditions



Isothermal at 300 K.

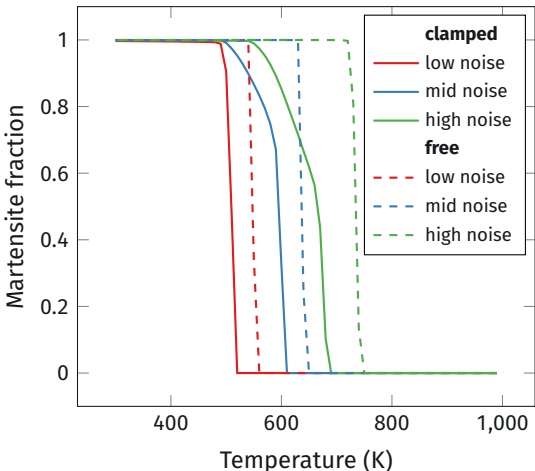


Free: fully martensitic, finer microstructure.

Clamped: 2 % retained austenite, coarser microstructure.

Nucleation is easier in the free case: more nuclei → finer microstructure.

Benchmark simulations: influence of boundary conditions and noise amplitude on martensite fraction

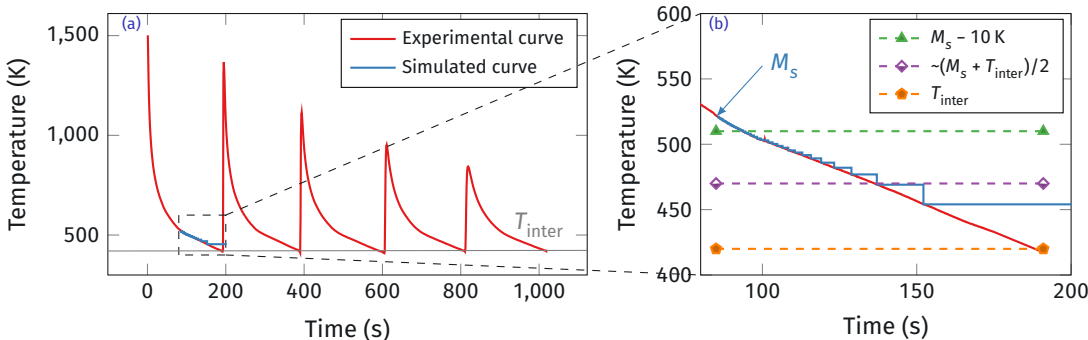


- Martensite fraction % α' :

- free: $M_s \approx M_f$
- clamped: $M_s \neq M_f$
(close to KOISTINEN-MARBURGER relation).
- Higher noise \rightarrow higher M_s .

Selection of clamped elastic boundaries to study the partitioning of carbon between martensite and austenite.

Simulations of *real* thermal cycle: first quenching during WAAM



(a) Experimental cooling curve from air-quenching of ER410 NiMo steel during WAAM. (b) Zoom of delimited zone in (a) and isothermal simulations.

- 4 simulations:**
- 1 **coupled** simulation starting at M_s
 - 3 **isothermal** simulations at characteristic temperatures.

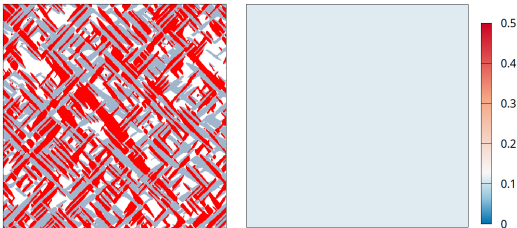
Is partitioning going to occur during quenching ?

Simulations using the experimental cooling curve

coupled simulation

Martensite map

X_C (at.%C)



Microstructure and carbon content (carbon fraction)
evolution during the coupled simulation.

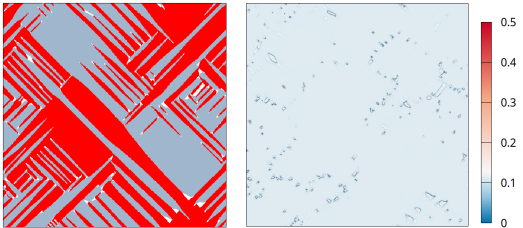
- Start (521 K).
- Middle of cooling curve (504 K).
- End of curve (454 K).

Simulations using the experimental cooling curve

coupled simulation

Martensite map

X_C (at.%C)



Microstructure and carbon content (carbon fraction)
evolution during the coupled simulation.

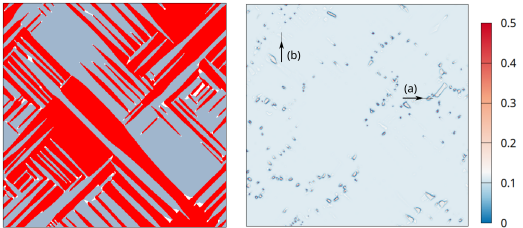
- Start (521 K).
- Middle of cooling curve (504 K).
- End of curve (454 K).

Simulations using the experimental cooling curve

coupled simulation

Martensite map

X_C (at.%C)



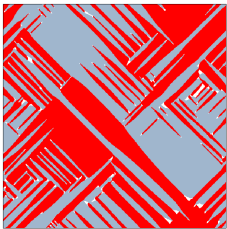
Microstructure and carbon content (carbon fraction)
evolution during the coupled simulation.

- Start (521 K).
- Middle of cooling curve (504 K).
- End of curve (454 K).

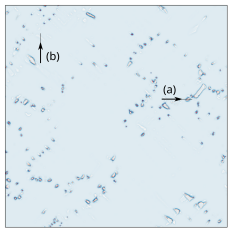
Simulations using the experimental cooling curve

coupled simulation

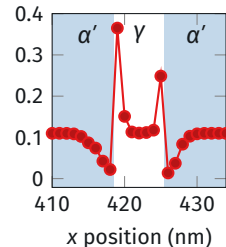
Martensite map



X_C (at.%C)

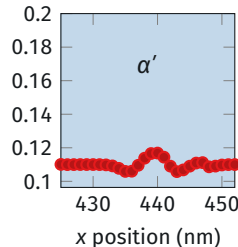


Carbon content (at.%C)



(a) Profile at the α'/γ interface from line (a).

Carbon content (at.%C)



(b) Profile through a former austenitic domain from line (b).

Microstructure and carbon content (carbon fraction) evolution during the coupled simulation.

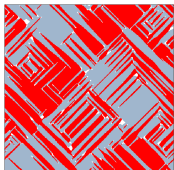
- Start (521 K).
- Middle of cooling curve (504 K).
- End of curve (454 K).

- **Carbon segregated during quenching.**
- **Establishment of asymmetrical composition profiles at α'/γ boundaries.**
- **Persistent traces of previous segregation in now fully martensitic zones.**

Simulations using the experimental cooling curve

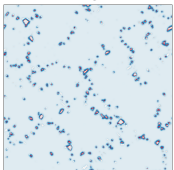
comparison with isothermal simulations

Martensite

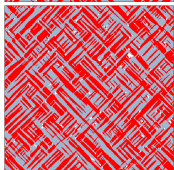


510 K

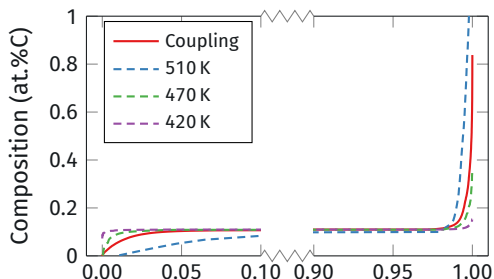
X_C (at.%C)



470 K



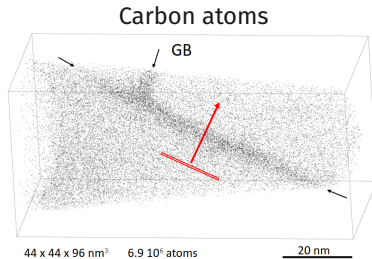
420 K



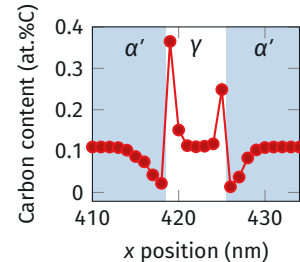
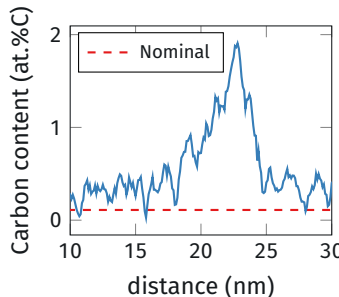
Cumulated frequencies of carbon composition for coupled and isothermal simulations.

- Martensite is finer when T_{step} is lower because of nucleation.
- Isothermal simulation **over or under** estimate the segregations.
- **Too many assumptions have to be made (T_{step} , Δt_{step}) for the isothermal simulations compared to the coupled one.**

Comparison between coupled simulation and experimental sample



Experimental (APT) atomic composition profile through an interface inside the martensite.



Carbon concentration profile from the coupled simulation.

Consistency between simulation and experimental sample subjected to **same cooling curve**:

- **similar enrichment amplitude (~ 10x the nominal composition)**
- **similar diffusion distance (~ 5 nm).**

Contents

1 Introduction

2 Phase-field method

- Order parameters
- Energy of the system
- Coupling strategy

3 Results

- Benchmark simulations
- Simulations using the experimental cooling curve from WAAM

4 Conclusion

Conclusions & perspectives

Conclusions

- Study of the microstructure of a martensitic stainless steel during WAAM.
- Proposition of a novel **displacive/diffusive coupling**.
- *Explicit CALPHAD* description of the phases for temperature and composition dependence.
- Replication of KOISTINEN-MARBURGER curves with M_s and M_f temperatures.
- Comparable carbon segregation between the coupled simulation and an experimental sample subjected to **the same** cooling curve.
- Persistent traces of previous carbon segregation in fully martensitic zones, which can only be obtained with this coupling strategy.

Perspectives

- Testing the impact of other carbon composition.
- Study the effect of cooling speed on retained austenite fraction.



MMM11 - symposium O

Phase-field modelling of microstructure evolution during complex thermal cycles : application to martensitic steels

Jules L'HOSTIS*, Marie-Noëlle AVETTAND-FÈNOËL, Manon
BONVALET-ROLLAND and Ludovic THUINET

Univ. Lille, CNRS, INRAE, Centrale Lille, UMR 8207 - UMET - Unité Matériaux et
Transformations, F-59000 Lille, France

September 26th, 2024



*jules.l_hostis@centralelille.fr



Thank you for your attention !

Please, feel free to ask any questions.

-

Jules L'HOSTIS
jules.l-hostis@univ-lille.fr

This work was funded by the Région Hauts de France and Centrale Lille.

References

- [1] P. G. Kubendran Amos, E. Schoof, N. Streichan, D. Schneider, B. Nestler, *Computational Materials Science* **2019**, 159, 281–296.
- [2] D. H. Sherman, S. M. Cross, S. Kim, F. Grandjean, G. J. Long, M. K. Miller, *Metallurgical and Materials Transactions A* **2007**, 38, 1698–1711.
- [3] H. K. Yeddu, A. Malik, J. Ågren, G. Amberg, A. Borgenstam, *Acta Materialia* **2012**, 60, 1538–1547.
- [4] A. G. Khachaturyan, *Theory of Structural Transformations in Solids*, 1983.
- [5] W. Liu, C. Chen, Y. Tang, Q. Long, S. Wei, G. Zhang, F. Mao, Q. Jiang, T. Zhang, M. Liu, *Calphad* **2020**, 69, 101763.

Interlath segregation

Because of the asymmetrical profile of $G_v^{\text{chem}}(\eta)$, at the interface between martensite variants, $\sum_p \eta_p \neq 1$, which is non-physical and attracts carbon.

A condition is added to consider the α'/α' interface as martensite:

$$\begin{cases} \frac{\partial G_v^{\text{chem}}}{\partial X_C} = \frac{\partial G_v^{\alpha'}}{\partial X_C} & \text{if } \forall gp \frac{\partial G_v^{\text{grad}}}{\partial \eta_{gp}} > 0.03 \\ \frac{\partial G_v^{\text{chem}}}{\partial X_C} = -\left(\frac{\partial G_v^{\alpha'}}{\partial X_C} - \frac{\partial G_v^\gamma}{\partial X_C}\right)\left(4\sum_{gp} \eta_{gp}^3 - 3\left(\sum_{gp} \eta_{gp}^2\right)^2\right) + \frac{\partial G_v^\gamma}{\partial X_C} & \text{otherwise} \end{cases} \quad (9)$$

Mobility coefficient determination

The inhomogeneous mobility coefficient is given by a mixing law:

$$M(\mathbf{r}, t) = M^{\alpha'}(T) \left(\sum_{gp} \eta_{gp}^2 \right) + M^Y(T) \left(1 - \sum_{gp} \eta_{gp}^2 \right) \quad (10)$$

and the mobility coefficient of carbon in the different phases can be calculated with:

$$M^\phi(T) = D^\phi(T) \left(\frac{\partial^2 G_v^\phi}{\partial X_c^2} \right)^{-1} \quad (11)$$

with $D^\phi(T)$ the diffusion coefficients, which are calculated by⁸:

$$D^Y = 4.53 \times 10^{-7} \left(1 + y_c^{(2)} \left(1 - y_c^{(2)} \right) \frac{8339.9}{T} \right) \cdot \exp \left(- \left(\frac{1}{T} - 2.21 \times 10^{-4} \right) \left(17767 - 26436 y_c^{(2)} \right) \right) \quad (12)$$

$$D^{\alpha'} = 0.02 \times 10^{-4} \cdot \exp \left(\frac{-10115}{T} \right) \cdot \exp \left(0.5898 \left(1 + \frac{2}{\pi} \arctan \left(1.4985 - \frac{15309}{T} \right) \right) \right) \quad (13)$$

⁸P. G. Kubendran Amos et al., *Computational Materials Science* **2019**, 159, 281–296.

Experimental plan and parameters selection

- Isothermal simulations:
 - Verify the martensitic features.
- Continuous cooling:
 - Choose elastic boundary conditions.
- displacive/diffusive coupling:
 - Compare with experimental sample.

Physical parameters.

Carbon content	X_C	0.11 at.%C
Martensite start T	M_s	521 K
Interfacial energy	Γ	0.08–0.2 J · m ⁻²
Stress free strain (SFT) ⁹	ϵ_1 / ϵ_3	0.136 / -0.087

⁹Coefficients were modified to preserve the 3D volume expansion in 2D.

List of constant parameters, (*) means dimensionless.

Parameter	Symbol	Value
<i>General</i>		
Box size		512 × 512 cells
Cell size	a_0	1.0 nm
Gradient coefficient	κ^*	10
Displacive time	Δt_m^*	3.71×10^{-4}
Diffusivetime	Δt_d^*	3.71×10^{-7}
Displacive step length		10×10^3 iterations
Room temperature		300 K
<i>Noise</i>		
Noise cutout		10 % of step
Noise frequency		1/50
<i>Elasticity</i>		
Elastic constants	C_{11}^*	9.81×10^3
	C_{12}^*	5.89×10^3
	C_{44}^*	1.96×10^3
OP stabilization range	ϵ	0.1